Entrainment and modulation of nonlinear dissipative waves under external forcing(Mathematical modeling and analysis for nonlinear phenomena)

AUTHOR(S):

Tokuda, Hidekazu; Ohta, Takao

CITATION:

Tokuda, Hidekazu ...[et al]. Entrainment and modulation of nonlinear dissipative waves under external forcing(Mathematical modeling and analysis for nonlinear phenomena). 数理解析研究所講究録 2006, 1522: 1-13

ISSUE DATE:

2006-10

URL:

http://hdl.handle.net/2433/58814

数理解析研究所講究録
1522 巻 2006 年 1-13

Entrainment and modulation of nonlinear dissipative waves under external forcing

Hidekazu Tokuda and Takao Ohta
Yukawa Institute for Theoretical Physics, Kyoto University, Kyoto 606-8502, JAPAN

INTRODUCTION

Various self-organized patterns emerge in non-equilibrium open systems. Spatio-temporal properties of these patterns have been studied extensively both experimentally and theoretically for many years. For example, mathematical theories for spiral waves in Belousov-Zhabotinsky reaction have been developed [1]. Reduction methods to represent pattern dynamics have also been developed [2, 3]. The interaction between localized objects in nonlinear dissipative systems has been formulated [4].

The effects of external forcing in pattern dynamics have also been studied. One of the typical problems is synchronization of nonlinear oscillators with an externally applied periodic disturbance [1, 5]. This is an example of nonlinear response in a nonequilibrium steady state, which should be developed further in biophysics such as dynamics of collective network in biological cells. Another reason as to why the effects of external forcing is interested is that it might be useful to control the mesoscopic structures in material sciences. In fact, there are interesting experiments of domain dynamics in chemical reactions adsorbed on metal surfaces [6] and in nonequilibrium monolayers [7–10].

Here we mention several older studies related to the subjects in the present paper. Experiments of convective nematic fluids under spatially periodic forcing have been performed [11] and a theoretical study has been available [12]. Influence of temporal modulation on pattern formation has been investigated in convective fluids [13–15] and in chemical reactions [16, 17]. Quite recently, experiments and theoretical consideration have began for Turing patterns influenced by spatio-temporal forcing. For example, effects of illuminating light on spatially periodic structures and on spiral waves are investigated in chemically reacting systems [18–21].

The purpose of the present paper is to investigate, theoretically and by numerical simulations, dynamics of traveling waves under spatio-temporal external forcing. In our previous paper, we introduced a model set of equations for phase separated mixtures undergoing chemical reactions [22, 24] and studied synchronization and modulation of motionless and propagating waves in two dimensions by applying spatially uniform oscillating external disturbance [23]. The external forcing was imposed by allowing one of the reaction rates space-time dependent. Here we generalize this study to the case of spatio-temporal external forcing and carry out numerical simulations in one dimension and develop a theoretical analysis to understand the results of simulations.

To our knowledge, despite the previous studies mentioned above, response of propagating periodic structures to the space-time dependent external disturbance has not been explored until recently. Zykov et.al. [25] have investigated spiral wave under traveling wave modulation. In our previous paper [26], we studied propagating waves under spatio-temporal modulations and considered the case that the spatial period of the external forcing is the same as the intrinsic period of the traveling waves. The present paper deals with the case where there is a small misfit between the two periods. A part of the preliminary results has been reported in ref. [27]

The organization of the present paper is as follows. In the next section, we start with a brief explanation of the model system and introduce the external forcing. To make the present paper self-contained, the results of the linear stability analysis obtained previously [26] are also described. In section 3, we present localized modulation of traveling waves under incommensurate external forcing. The special case where the external frequency is equal to zero, i.e, motionless external forcing is investigated both numerically and theoretically in section 4. Discussion is given in section 5 including an analysis of mode selection of the propagating waves.

MODEL EQUATION AND EXTERNAL FORCING

In our previous papers [22–24], we introduced a hypothetical chemical reaction with three chemical components A, B and C

$$A \xrightarrow{\gamma_1} B \xrightarrow{\gamma_2} C \xrightarrow{\gamma_3} A \tag{1}$$

with the reaction rates γ_1, γ_2 and γ_3. We assume that other components are also involved in the chemical reaction, which are supplied to the system and removed from the system sufficiently rapidly so that they are constant in both

space and time. Therefore these components modify only the reaction rates. The reason as to why we consider the cyclic chemical reaction is that the system is maintained far from equilibrium.

In order to realize a spatial order as well as temporal order, we assume that A and B species tend to segregate each other at low temperatures and the component C is neutral both to A and B components. By introducing the local concentrations ψ_A, ψ_B and ψ_C of A, B and C components respectively, the time-evolution equations are given by [22]

$$\frac{\partial \psi}{\partial t} = \nabla^2 \frac{\delta F}{\delta \psi} + f(\psi, \phi), \tag{2}$$

$$\frac{\partial \phi}{\partial t} = g(\psi, \phi), \tag{3}$$

where $\psi = \psi_A - \psi_B$ and $\phi = \psi_A + \psi_B$. We have imposed the condition $\psi_A + \psi_B + \psi_C = 1$ which is justified by the assumption of the uniformity of other chemical species as mentioned above. The free energy functional F is given by

$$F = \int d\mathbf{r} \left[\frac{D}{2} (\nabla \psi)^2 - \frac{\tau}{2} \psi^2 + \frac{1}{4} \psi^4 \right], \tag{4}$$

where D and τ are positive constants. In this free energy, we have ignored, for simplicity, the coupling terms between ψ and ϕ. The last terms in eqs. (2) and (3) arise from the chemical reaction (1)

$$f(\psi, \phi) = -\left(\gamma_1 + \frac{\gamma_2}{2}\right) \psi - \left(\gamma_1 - \frac{\gamma_2}{2} + \gamma_3\right) \phi + \gamma_3, \tag{5}$$

$$g(\psi, \phi) = \frac{\gamma_2}{2} \psi - \left(\frac{\gamma_2}{2} + \gamma_3\right) \phi + \gamma_3. \tag{6}$$

Note that the diffusion term is not considered in eq. (3) because it does not alter essentially the dynamics described below [24].

The uniform stationary solution of eqs. (2) and (3) is readily obtained as

$$\psi_0 = \frac{\gamma_3(\gamma_2 - \gamma_1)}{\gamma_1\gamma_2 + \gamma_2\gamma_3 + \gamma_3\gamma_1}, \tag{7}$$

$$\phi_0 = \frac{\gamma_3(\gamma_2 + \gamma_1)}{\gamma_1\gamma_2 + \gamma_2\gamma_3 + \gamma_3\gamma_1}. \tag{8}$$

The linear stability of the uniform solution was carried out by putting $\psi - \psi_0 = c_1 \exp(\lambda t + iqx)$ and $\phi - \phi_0 = c_2 \exp(\lambda t + iqx)$ with c_1 and c_2 constants and by substituting these into eqs. (2) and (3). In this section, we fix the parameters as $D = 1$, $\gamma_1 = 0.3$ and $\gamma_3 = 0.05$ and the remaining two parameters τ and γ_2 are varied. At some range of the parameters, the eigenvalue λ is found to be complex. An example is shown in Fig. 1 for $\tau = 1.46$ and $\gamma_2 = 0.16$ as a function of wave number. Note that the real part becomes positive at a finite wave number q_c and the imaginary part has a minimum at $q = q_c$.

The expressions of q_c, τ_c and the critical frequency ω_c which is the imaginary part of the eigenvalue at $q = q_c$ are given for $\tau > 3\psi_0^2$ by

$$q_c = \left(\frac{\tau - 3{\psi_0}^2}{2}\right)^{1/2}, \tag{9}$$

$$\tau_c = 3{\psi_0}^2 + 2(\gamma_1 + \gamma_2 + \gamma_3)^{1/2}, \tag{10}$$

$$\omega_c = \left(\frac{\gamma_1\gamma_2 - \gamma_2\gamma_3 - {\gamma_2}^2}{2} - {\gamma_3}^2\right)^{1/2}. \tag{11}$$

The linear stability analysis gives us the bifurcation diagram shown in Fig. 2 [24]. A motionless periodic pattern appears in the region indicated by $\times$ in Fig. 2 whereas a propagating wave pattern appears in the region $+$. The

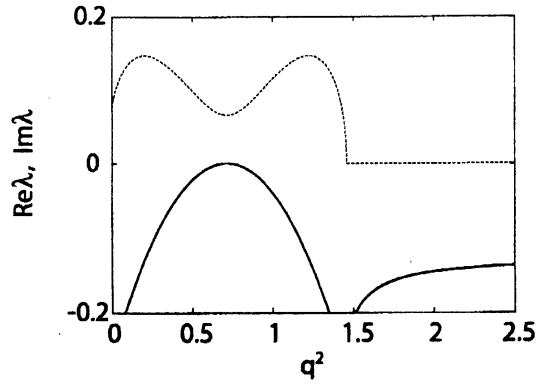

FIG. 1: The wave-number dependence of Re λ(q) (solid line) and Im $\lambda(q)$ (dashed line) for $D = 1.0, \tau = 1.46, \gamma_1 = 0.3, \gamma_2 = 0.16$ and $\gamma_3 = 0.05$.

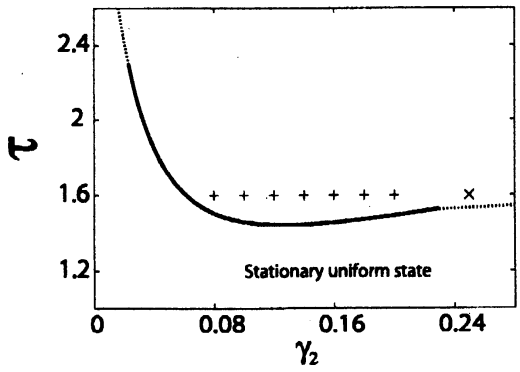

FIG. 2: Bifurcation diagram for the uniform stationary solution for $D = 1$, $\gamma_1 = 0.3$ and $\gamma_3 = 0.05$. The full line and the dotted line are the Hopf bifurcation line and the Turing-type bifurcation line respectively. A traveling wave appears at the parameters indicated by the symbol + whereas a motionless pattern at the symbol ×.

value of τ at the Hopf bifurcation point for $\gamma_2 = 0.16$ is $\tau_c \approx 1.46$ at which the critical wave number is $q_c \approx 0.85$ and the critical frequency $\omega_c \approx 0.07$.

In order to study the behavior above the bifurcation lines we have carried out numerical simulations of eqs. (2) and (3) in one dimension. The Euler method is employed with the system size $L = 64$, the mesh size 0.5 and the time increment 0.001 and a periodic boundary condition is imposed.

Figure 3 displays the spatial variation of a propagating wave. Since eqs. (2) and (3) are invariant under the transformation $x \to -x$, the traveling wave can propagate either to the right or to the left with a certain phase difference between ϕ and ψ. Hereafter we choose (with an appropriate initial condition) a wave traveling to the right without loss of generality.

The spatio-temporal forcing is introduced as follows. We suppose that the system is exposed through periodically arrayed slits by illuminating light and the slit moves at a constant velocity Ω/q_f with $2\pi/q_f$ the period of the slits. As a result, we assume that the reaction rate γ_3 is modified such that $\gamma_3 \to \gamma_3 + \Gamma$ where Γ represents the effect of illumination. We shall ignore a term $\Gamma\phi$ arising from the $\gamma_3\phi$ term in eqs. (5) and (6) providing a sufficiently small forcing ϵ. In this way, the set of equations (2) and (3) has an additive term

$$\Gamma(x,t) = \epsilon \cos(q_f x - \Omega t). \tag{12}$$

This is a sinusoidal force traveling to the right at the velocity Ω/q_f.

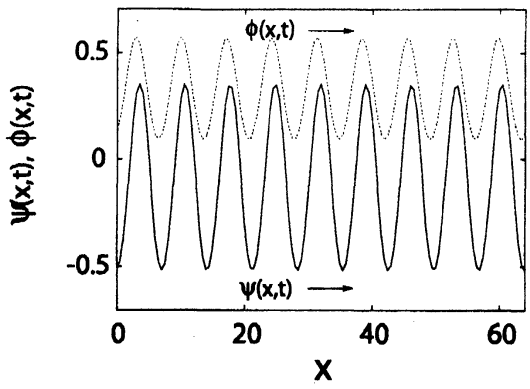

FIG. 3: Spatial profiles of $\psi(x,t)$ (solid line) and $\phi(x,t)$ (dashed line) for $D = 1.0, \tau = 1.6, \gamma_1 = 0.3, \gamma_2 = 0.16$ and $\gamma_3 = 0.05$. Both $\psi(x,t)$ and $\phi(x,t)$ are propagating to the right at the same velocity.

LOCALIZED MODULATION OF TRAVELING WAVES

We have carried out numerical simulations of eqs. (2) and (3) with the external force (12). When the external forcing is present, the system size is set to be $L = 2\pi N/q_f$ and q_f is varied from 0.2 to 1.6. The integer number N is changed with q_f as $N = 10q_f$ so that the system size is always equal to $L = 20\pi$. Note that the intrinsic wave number is given by $q_c \approx 0.9$ for $\tau = 1.6$ and $\gamma_2 = 0.16$. (We shall not use the value of $q_c = 0.85$ at the bifurcation point $\tau_c = 1.46$ but use the value at $\tau = 1.6$ where numerical simulations will be carried out.) Note also that L is approximately commensurate with $2\pi/q_c$, i.e., $Lq_c/2\pi \approx 9$.

The traveling wave solution is provided without the external forcing, then the forcing term is turned on and examine the asymptotic behavior. Figure 4 summarizes the behavior on the $\Omega - q_f$ plane for the parameters $\gamma_1 = 0.3$, $\gamma_2 = 0.16$, $\gamma_3 = 0.05$, $\tau = 1.6$ and $\epsilon = 0.006$. As mentioned above, the critical wave number is $q_c \approx 0.9$ and the critical frequency $\omega_c \approx 0.07$. There is a region indicated by + around $q_f = q_c$ and $\Omega = \omega_c$ where the traveling wave is entrained with the external force, as expected, so that it propagates at the velocity Ω/q_f as in Fig. 5(a). When the frequency Ω of the external forcing is far away from ω_c but $q_f = q_c$ as in the region indicated by the diamond symbols, entrainment breaks down and the traveling wave is modulated such that the amplitude as well as the propagating velocity is uniformly oscillating. When the velocity is decreased, the amplitude is also decreased and vice versa as shown in Fig. 5(b). This uniform modulation was studied in detail in the previous paper [26].

Next, we show the case that the wave length of the trains is different from the spatial period of the external forcing, i.e., $q_f \neq q_c$. When the external frequency Ω and the external wave number q_f are much different from ω_c and q_c, the traveling wave is modulated both in space and time. The essential difference from the case of $q_f = q_c$ is that the modulation is localized in space. A snapshot of the concentration profiles of ψ is displayed in Fig. 6. It is noted that the envelop of the amplitude is localized as indicated by the arrow. The propagating direction of the locally modulated region depends on the parameters. In fact, it propagates to the left in Fig. 7(a) in the parameter region of the white circles in Fig. 4 whereas the localized modulation propagates to the right in Fig. 7(b) in the region indicated by the black circles in Fig. 4.

We have not fully succeeded in formulating the localized modulation for $q_c \neq q_f$. Here we describe a simple argument to understand the velocity of the localized region. The velocity of the external forcing is given by $v_f = \Omega/q_f$ and the velocity of the traveling wave near the bifurcation threshold in the absence of the external forcing is defined by $v_c = \omega_c/q_c$. First we consider the case $v_f > v_c$ and $q_f > q_c$. Let us suppose that the variable $\psi(x,t)$ and the external forcing $\Gamma(x,t)$ are in phase at the point A and $t = 0$ as indicated in Fig. 8. This point A traverses at the distance $v_c T$ during a certain interval T. The point B of Γ in Fig. 8 catches up the point A at the point C if T satisfies

$$Tv_f = 2\pi/q_f + Tv_c. \tag{13}$$

During this period, the localized region propagates the whole system plus Tv_c so that its velocity v_L has to satisfy

$$Tv_L = N_f 2\pi/q_f + Tv_c. \tag{14}$$

where $N_f = Lq_f/2\pi$ is the number of wave trains of the external forcing. Eliminating T from (13) and (14), one

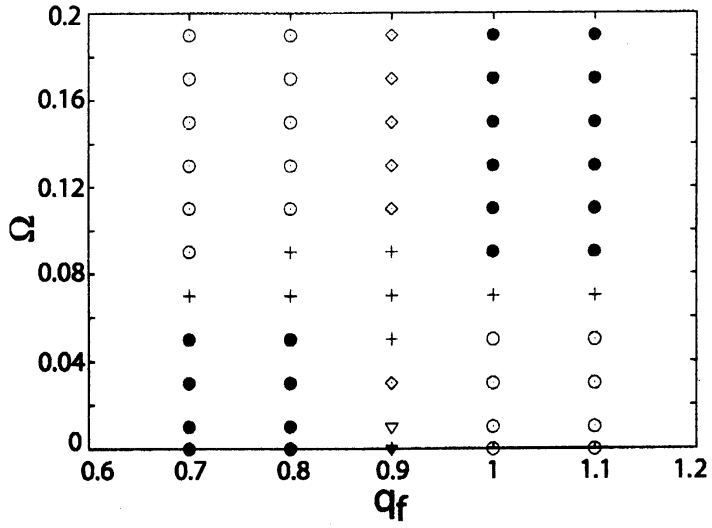

FIG. 4: Phase diagram of modulation for $q_f \neq q_c$ and for the parameters $\gamma_1 = 0.3$, $\gamma_2 = 0.16$, $\gamma_3 = 0.05$, $\tau = 1.6$ and $\epsilon = 0.006$. At the region indicated by the plus symbols around $q_c = 0.9$ and $\omega_c = 0.07$ the waves are entrained with the external forcing. At the region indicated by the diamond symbols for $q_c = 0.9$ a uniform oscillation of modulation occurs. The localized modulation appears at the region indicated by the black (white) circles where the localized region propagates to the right (left).

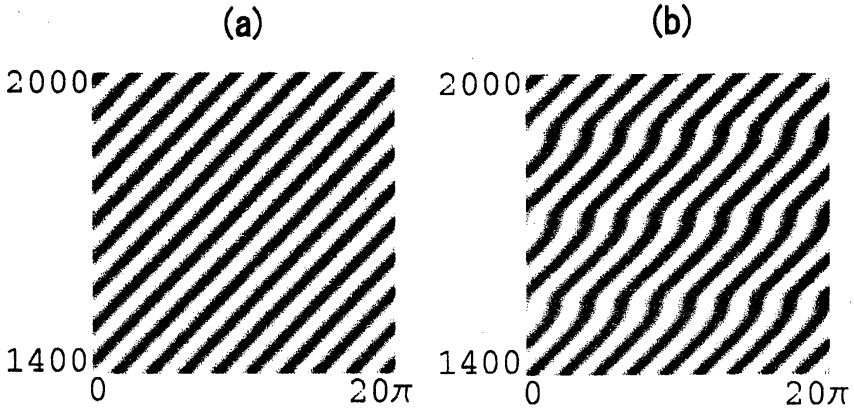

FIG. 5: Space (horizontal)-time (vertical) plot of ψ for (a) $q_f = 0.9$ and $\Omega = 0.09$, and (b) $q_f = 0.9$ and $\Omega = 0.11$. The value of ψ is large (small) for lighter (darker) regions. No modulation appears in (a). The modulation occurs periodically in time but uniformly in space in (b).

obtains

$$v_L = N_f(v_f - v_c) + v_c. \tag{15}$$

It is readily found that this relation can be extended to the case $v_f < v_c$. In the case of $q_f < q_c$, a similar argument gives us

$$v_L = (N_f + 1)(v_c - v_f) + v_f. \tag{16}$$

These theoretical results are compared with simulations in Figs. 9 for (a) $q_f = 1.0$ and (b) $q_f = 0.8$. It is noted that the theoretical results are in a good agreement with the simulations for $\Omega > \omega_c = 0.07$. However, there is a small

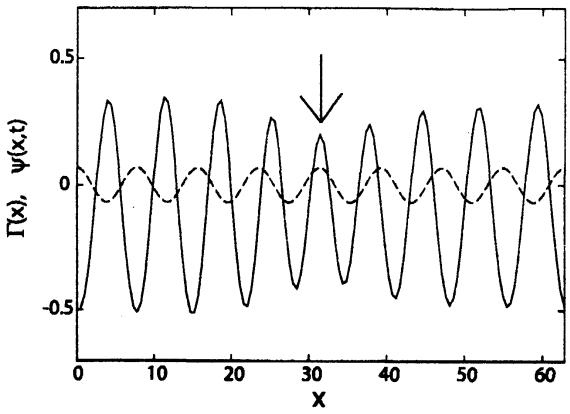

FIG. 6: Spatial profiles of $\psi(x,t)$ (solid line) and $\Gamma(x)$ (dashed line) for $D = 1.0, \tau = 1.6, \gamma_1 = 0.3, \gamma_2 = 0.16$, $\gamma_3 = 0.05$, $\epsilon = 0.007$, $\Omega = 0.0$ and $q_f = 0.8$. Both $\psi(x,t)$ and a localized modulation (indicated by arrows) are propagating to the right.

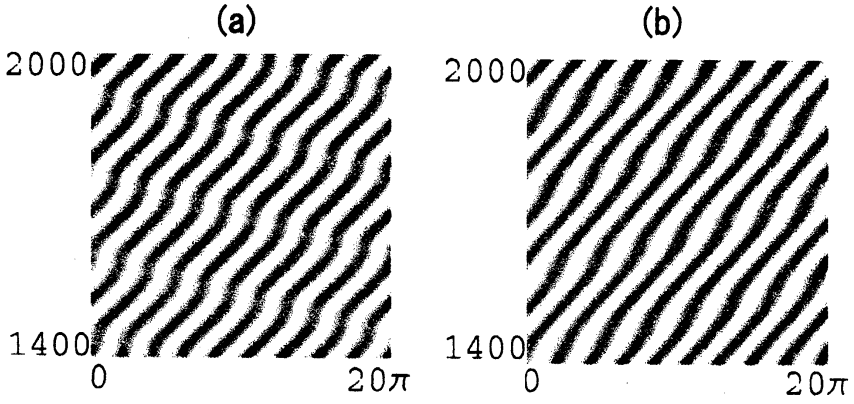

FIG. 7: Space (horizontal)-time (vertical) plot of ψ for (a) $q_f = 0.8$ and $\Omega = 0.11$ and (b) $q_f = 1.0$ and $\Omega = 0.11$. The value of ψ is large(small) for lighter (darker) regions. The localized modulation propagates to the left in (a) and to the right in (b).

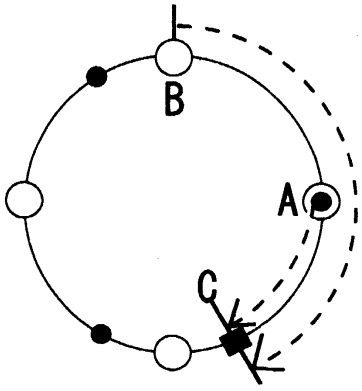

FIG. 8: Relative configuration of the wave $\psi(x,t)$ and the external force $\Gamma(x,t)$. The locations of maxima of the periodic ψ are shown by the black circle whereas those of Γ are by the white circles.

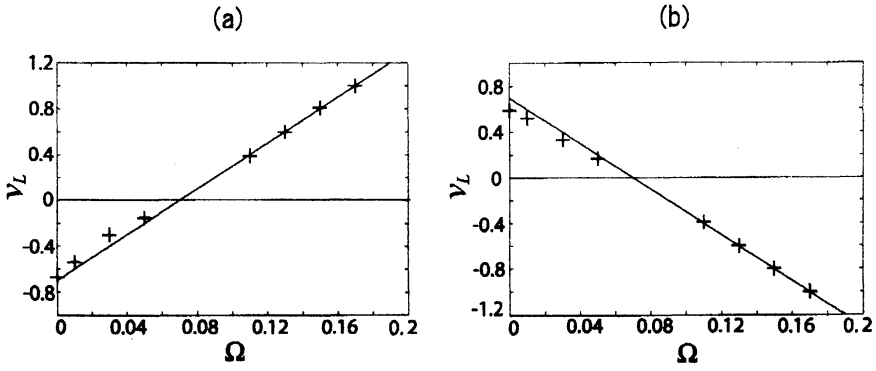

FIG. 9: Ω-dependence of the velocity v_L of the localized modulation for (a) $q_f = 1.0$ and (b) $q_f = 0.8$. The results of simulations given by the symbol + are compared with the theoretical results eq. (15) in (a) and eq. (16) in (b). Note that the velocity is defined to be positive when the localized modulation is propagating to the right.

but systematic deviation between them for smaller values of Ω. In fact, the absolute value of v_L is smaller than the theoretical value. As is seen in Fig. 8, the above argument assumes implicitly the distortion of the wave due to the external forcing is small. The results indicate that the coupling between the external forcing and the propagating wave is stronger when the velocity of the external forcing is small, i.e., $\Omega < \omega_c$. This is qualitatively understood because the effect of the periodic external force is smeared out when the velocity is large enough.

LOCKED STATE FOR $\Omega = 0$ AND ITS STABILITY

In this section, we fix the external frequency as $\Omega = 0$ and the remaining two parameters ϵ and q_f are varied. The results are shown on the $\epsilon - q_f$ plane in Fig. 10 and Fig. 11. When the external forcing ϵ is sufficiently large and near $q_f = q_c = 0.9$ as indicated by the plus symbols, the waves are locked by the external forcing. In other regions modulation of waves is observed. The localized modulation occurs and propagates to the right in the region indicated by the black circles whereas it propagates to the left in the region indicated by the white circles. In the region indicated by the black triangles waves undergo a coherent in-phase oscillation in the confined interval of one wavelength of the external force. In the region indicated by the squares, more complicated oscillatory motions appear as described in detail below.

The representative motions of waves are shown in space-time plot in Figs. 12, 13 and 14. Figure 12 displays the results for $q_f = q_c = 0.9$. When ϵ is sufficiently small, a periodic modulation appears as Fig. 12(a), which is essentially the same as that in Fig. 5(b). When the magnitude of ϵ is intermediate, the waves undergo a trapped in-phase oscillation as Fig. 12(b). The waves are locked (frozen) by the external forcing for sufficiently large values of ϵ as indicated in Fig. 12(c). These were obtained and analyzed in the previous paper [26].

When $q_f = 0.6$ a localized modulation propagating to the right appears for small values of ϵ whereas the waves are locked for large values of ϵ as clearly seen in Figs. 13(a) and (c). An oscillatory dynamics shown in Fig. 13(b) is observed in the small interval between these two behavior. Note that this oscillation is similar to but different from the trapped oscillation mentioned above. In fact the motion of a pair of the adjacent domains is anti-phase. The reason of the anit-phase oscillation can be understood qualitatively as follows. When $q_f = 0.6$, there are 6 ($= 10q_f$) trains of the external forcing. On the other hand, the intrinsic number of propagating wave trains is 9 ($= Lq_c/2\pi$ for $q_c = 0.9$). This means that there are three clusters, each of which consists of three trains. These three trains survive equally for small values of ϵ but one of the trains (say, the middle one) tends to be eliminated by the external force for large values of ϵ. This conflict makes the other two trains anti-phase oscillation.

Figure 14 displays the results for $q_f = 1.2$. It is interesting to see that there is again a narrow region between the state of the localized modulation and the locked state, where an oscillatory state appears as in Fig. 14(b). Note, however, that the oscillation is more complicated in its spatial structure compared with the other two, i.e., Fig. 12(b) and Fig. 13(b). In this case the number of the trains of the external force is 12 whereas the intrinsic wave trains is 9. Therefore the waves trains make three clusters which contains three wave trains. When the external force ϵ is large, one more wave train tends to be produced in each cluster. This is possible only when the amplitude of the three wave

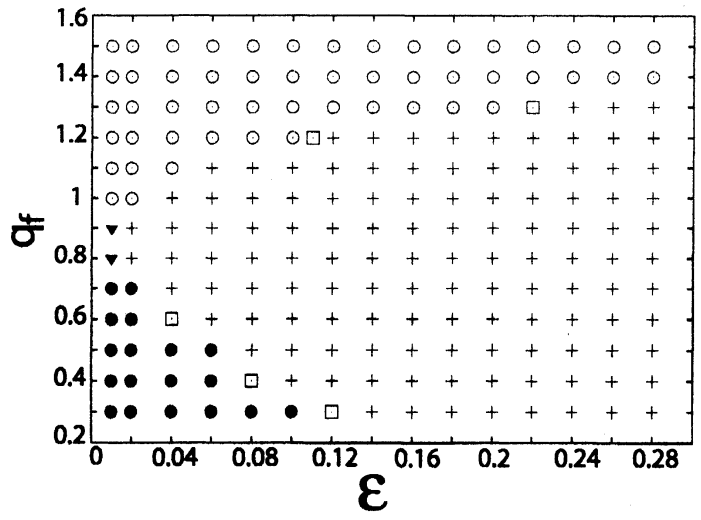

FIG. 10: Phase diagram for $\Omega = 0$, $\gamma_1 = 0.3$, $\gamma_2 = 0.16$, $\gamma_3 = 0.05$ and $\tau = 1.6$. In the plus region the waves are locked by the external force. In the region of the white (black) circles the localized modulation propagates to the left (right). In the regions indicated by the black triangles and the white squares, trapped oscillations of waves are observed. Those dynamics are shown in Figs. 12, 13 and 14 below.

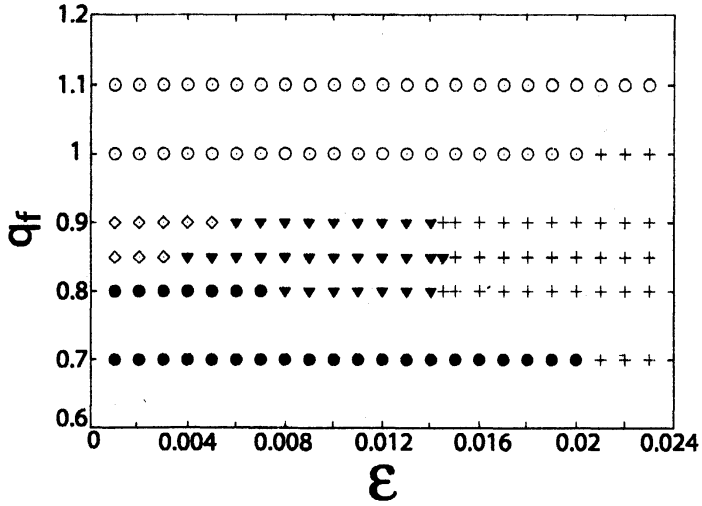

FIG. 11: Magnification of the phase diagram around $q_f = 0.9$ and $\epsilon = 0.01$. A periodic modulation occurs in the region indicated by the diamond symbols. The parameters are the same as those in Fig. 10.

trains is small. As a result, there is a standing oscillation of four wave trains such that the amplitude of the three wave trains is large but that of the fourth wave train is small and vice versa. This is actually happening in Fig. 14(b).

Here we develop a theory to understand the phase diagram near $q_f = q_c$ in Fig. 11. The following theory is an extension of our previous one [26] which was restricted only to the case $q_f = q_c$. The model equations (2) and (3) with the external forcing (12) can be written explicitly as

$$\begin{aligned} \frac{\partial \psi}{\partial t} &= \nabla^2 \left[-\nabla^2 \psi - \tau \psi + \psi^3 \right] + a_1 \psi + a_2 \phi \\ &+ \epsilon \cos(q_f x - \Omega t) + a_3, \end{aligned} \tag{17}$$

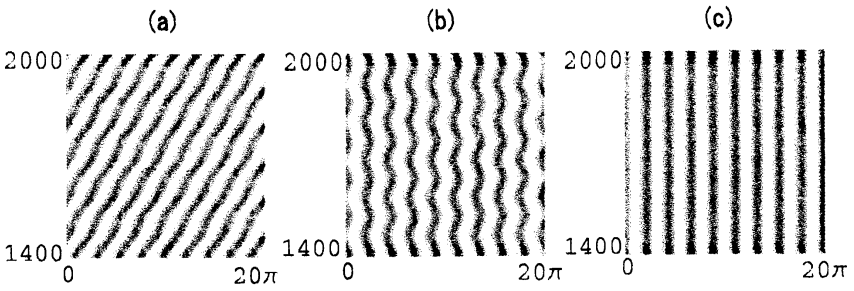

FIG. 12: Space (horizontal) -time (vertical) plot of ψ for $q_f = 0.9$ and for (a) $\epsilon = 0.005$, (b) $\epsilon = 0.01$ and (c) $\epsilon = 0.02$. Other parameters are chosen as $\Omega = 0$, $\tau = 1.6$ and $\gamma_2 = 0.16$.

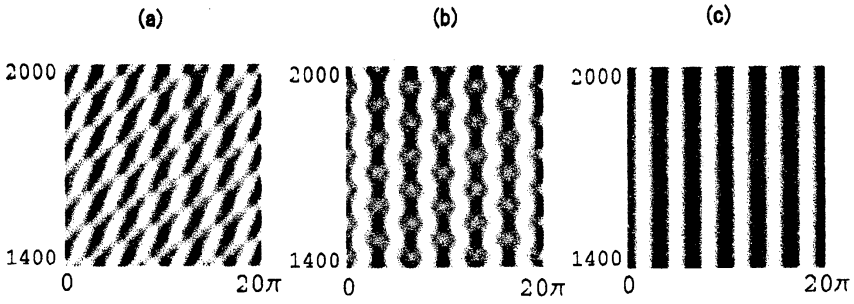

FIG. 13: Space (horizontal) -time (vertical) plot of ψ for $q_f = 0.6$ and for (a) $\epsilon = 0.036$, (b) $\epsilon = 0.04$ and (c) $\epsilon = 0.045$. Other parameters are the same as those in Fig. 12.

$$\frac{\partial \phi}{\partial t} = b_1 \psi + b_2 \phi + \epsilon \cos(q_f x - \Omega t) + b_3, \tag{18}$$

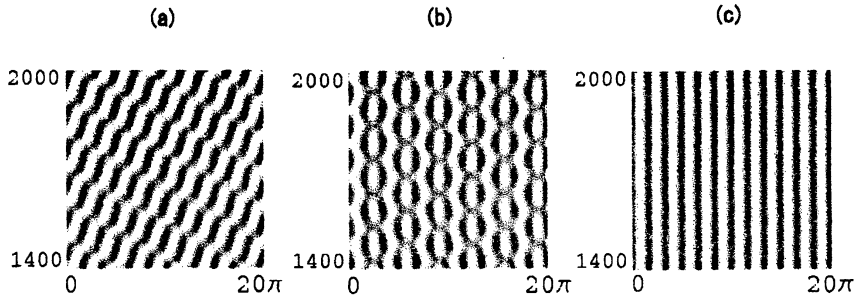

FIG. 14: Space (horizontal) -time (vertical) plot of ψ for $q_f = 1.2$ and for (a) $\epsilon = 0.1$, (b) $\epsilon = 0.115$ and (c) $\epsilon = 0.12$. Other parameters are the same as those in Fig. 12.

where

$$\begin{aligned} a_1 &= -\left(\gamma_1 + \frac{\gamma_2}{2}\right), \\ a_2 &= -\left(\gamma_1 - \frac{\gamma_2}{2} + \gamma_3\right), \\ a_3 &= \gamma_3, \\ b_1 &= \frac{\gamma_2}{2}, \\ b_2 &= -\left(\frac{\gamma_2}{2} + \gamma_3\right), \\ b_3 &= \gamma_3. \end{aligned} \tag{19}$$

The equilibrium uniform solutions ψ_0 and ϕ_0 have been given by eqs. (7) and (8).

Numerical simulations show that eqs. (17) and (18) have a motionless periodic solution for sufficiently large values of ϵ and those are well approximated by

$$\psi = \psi_0 + \bar{\psi}_1 \cos(q_f x), \tag{20}$$

$$\phi = \phi_0 + \bar{\phi}_1 \cos(q_f x), \tag{21}$$

We have veridied numerically that there is no phase difference between ψ, ϕ and the external force $\epsilon\cos(q_f x)$ and that $\bar{\psi}_1$ and $\bar{\phi}_1$ are negative. Substituting (20) and (21) into (2) and (3) and ignoring the higher harmonics generated by the nonlinear term, we obtain the set of equations for $\bar{\psi}_1$ and $\bar{\phi}_1$

$$-{q_f}^4\bar{\psi}_1 + \tau{q_f}^2\bar{\psi}_1 - {q_f}^2(3\psi_0^2\bar{\psi}_1 + \frac{3}{4}\bar{\psi}_1^3) + a_1\bar{\psi}_1 + a_2\bar{\phi}_1 + \epsilon = 0, \tag{22}$$

$$b_1\bar{\psi}_1 + b_2\bar{\phi}_1 + \epsilon = 0. \tag{23}$$

The neglect of the higher harmonics is justified as long as the sinusoidal deformation (20) and (21) holds which is indeed the case for the parameters considered here.

When the magnitude of the external force is decreased, the locked solution (20) and (21) becomes unstable as shown in Fig. 10. It is difficult to formulate the whole behavior in this Figure. We restrict ourselves to the region near $q = q_c = 0.9$ where a trapped oscillation appears after destabilization of the locked state as indicated in Fig. 11.

A trapped oscillation can be represented approximately by

$$\psi = \psi_0 + \bar{\psi}_1 \cos q_f(x + \theta_1(t)), \tag{24}$$

$$\phi = \phi_0 + \bar{\phi}_1 \cos q_f(x + \theta_2(t)), \tag{25}$$

where the time-evolution equations for the unknown phases $\theta_1(t)$ and $\theta_2(t)$ are to be derived. It consists of two steps. First substitute (24) and (25) into eqs. (17) and (18). Second, multiply each equation by $\sin q_f(x + \theta_1(t))$ and $\sin q_f(x + \theta_2(t))$ respectively and carry out the integral over one spatial period. In this way, we obtain

$$q_f\frac{d\theta_1}{dt} = c_1 \sin q_f(\theta_1 - \theta_2) + \epsilon_1 \sin(q_f\theta_1), \tag{26}$$

$$q_f\frac{d\theta_2}{dt} = -c_2 \sin q_f(\theta_2 - \theta_1) + \epsilon_2 \sin(q_f\theta_2), \tag{27}$$

where

$$c_1 = -\frac{a_2\bar{\phi}_1}{\bar{\psi}_1}, \qquad \epsilon_1 = -\frac{\epsilon}{\bar{\psi}_1} \tag{28}$$

$$c_2 = \frac{b_1\bar{\psi}_1}{\bar{\phi}_1}, \qquad \epsilon_2 = -\frac{\epsilon}{\bar{\phi}_1} \tag{29}$$

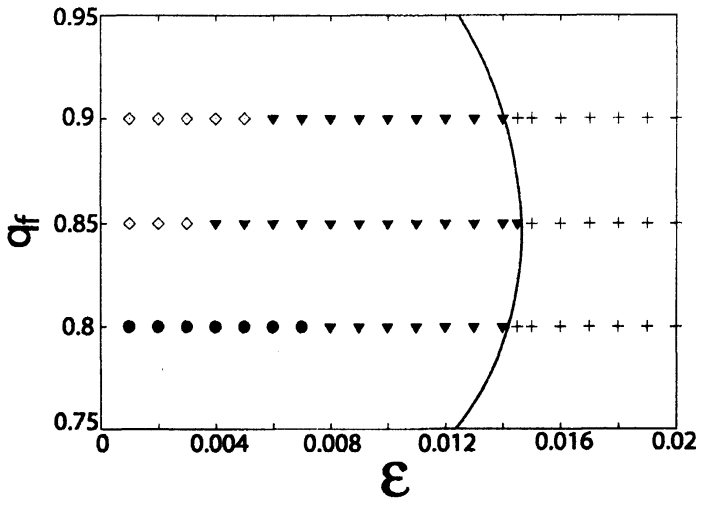

FIG. 15: Bifurcation diagram between the locked state and the trapped oscillation for $\Omega = 0$, $\gamma_1 = 0.3$, $\gamma_2 = 0.16$, $\gamma_3 = 0.05$ and $\tau = 1.6$. The solid line is the stability limit obtained theoretically. In the simulations for $q_f = 0.75$, 0.85 and 0.95, the system size is chosen as $L = 40\pi$ to make the external force commensurate with L. The meanings of the symbols are the same as those in Figs. 10 and 11.

Near the bifurcation threshold one may linearize these equations

$$\frac{d\theta_1}{dt} = c_1(\theta_1 - \theta_2) + \epsilon_1\theta_1, \tag{30}$$

$$\frac{d\theta_2}{dt} = c_2(\theta_1 - \theta_2) + \epsilon_2\theta_2, \tag{31}$$

The eigen value equation is readily obtained as

$$\lambda^2 - (c_1 + \epsilon_1 - c_2 + \epsilon_2)\lambda + c_1\epsilon_2 - c_2\epsilon_1 + \epsilon_1\epsilon_2 = 0 \tag{32}$$

The Hopf instability condition is given by

$$c_1 + \epsilon_1 - c_2 + \epsilon_2 > 0 \tag{33}$$

and

$$c_1\epsilon_2 - c_2\epsilon_1 + \epsilon_1\epsilon_2 > 0 \tag{34}$$

The solid line in Fig. 15 represents the above Hopf instability condition. Note that the theory agrees quite well with the simulation results.

The above theory was applied to the case $q_f = q_c$ in our previous paper [26]. What we have shown here is that it can also be applied successfully to the case $q_f \neq q_c$ as long as the difference is not too large.

DISCUSSION

We have studied dynamics of traveling waves under spatio-temporal forcing. When $q_f = q_c$, the behavior can be understood theoretically [26]. However, when $q_f \neq q_c$, more complex dynamics appears. In the present investigation, we have found propagating localized modulation, several different types of confined oscillations and the locked state. We have succeeded in predicting the velocity of the localized modulations which shows a good agreement with the simulations for the external frequency larger than the intrinsic frequency. The bifurcation from the locked state to the oscillatory state near $q_f = q_c$ is found to be understood by means of a phase dynamical approach.

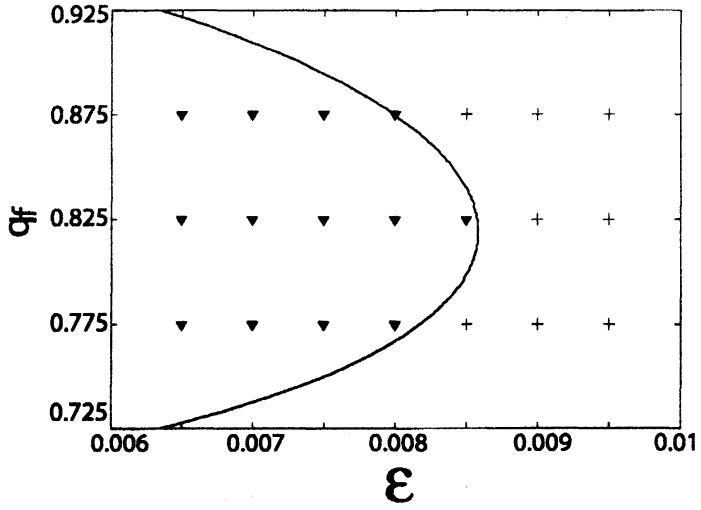

FIG. 16: Bifurcation diagram between the locked state and the trapped oscillation for $\gamma_2 = 0.1$, and $\tau = 1.55$. Other parameters are the same as those in Fig. 15. The solid line is the stability limit obtained theoretically. In these simulations the system size is chosen as $L = 80\pi$ to make the external force commensurate with L. The meanings of the symbols are the same as those in Figs. 10 and 11.

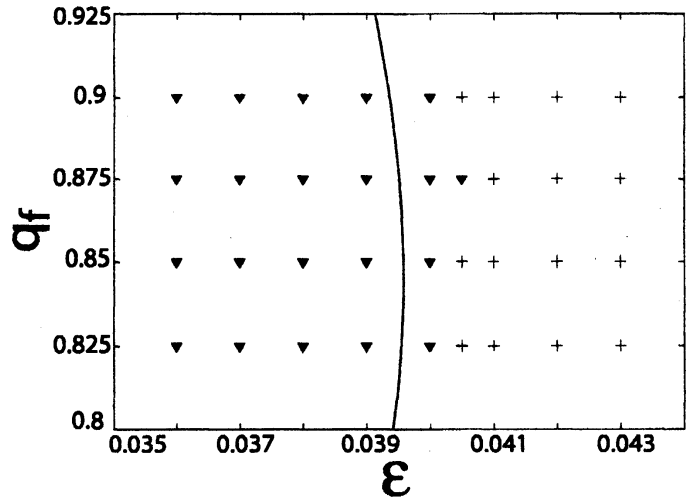

FIG. 17: Bifurcation diagram between the locked state and the trapped oscillation for $\gamma_2 = 0.16$, and $\tau = 2.5$. Other parameters are the same as those in Fig. 15. The solid line is the stability limit obtained theoretically. In these simulations the system size is chosen as $L = 80\pi$ to make the external force commensurate with L. The meanings of the symbols are the same as those in Figs. 10 and 11. The large discrepancy with the theory is not surprising because the theory ignores the higher harmonics and is valid only near the Hopf bifurcation $\tau = \tau_c = 1.46$.

What we have investigated in this paper is rather simple situation of the effects of external forcing. It is well known that the commensurate-incommensurate transition in thermal equilibrium exhibits a complicated phase diagram of various structures [28]. In this respect, even the locked state without propagation in the present problem is expected to be complicated enough by changing more widely the ratio q_c/q_f and the magnitude of the external force. More systematic approach is necessary for these aspects but it is left for a future study.

Finally we discuss about the mode selection in the present propagating waves. In pattern formation phenomena, to find a general principle for the mode selection beyond a bifurcation threshold is a fundamental unsolved problem

in non-variational dissipative systems. In this respect, it would be interesting to explore the possibility that some resonance condition might be related to the mode selection. That is, a periodic pattern might respond most strongly to an external periodic modulation whose period is the same as that of the intrinsic spatial period. In order to examine this possibility, we have carried out numerical simulations of traveling waves for sufficiently large system without external forcing. For example, we obtain the intrinsic wave number $q = 0.85$ of the propagating wave for $\gamma_2 = 0.16$ and $\tau = 1.6$. It is found from Fig. 15 that this wave number coincidences with the first wave number q_f where the locked state becomes unstable by decreasing ϵ and the trapped oscillation starts. We have also carried out numerical simulations for $\gamma_2 = 0.1$, and $\tau = 1.55$ and found that the intrinsic wave number is $q = 0.825$. This is also the first wave number of q_f as shown in Fig. 16. It is emphasized that this property is not limited near the bifurcation point of propagating waves. Figure 17 shows that the first wave number is $q_f = 0.875$ for $\tau = 2.5$ and $\gamma_2 = 0.16$. We have verified numerically that the intrinsic wave number of a propagating wave for these parameters is $q = 0.875$ for the system size $L = 80\pi$. (It is also true for these three cases that the wave number where the trapped oscillation appears in the widest interval of ϵ, e.g., $0.004 < \epsilon < 0.0145$ for $q_f = 0.85$ in Fig. 15 coincides with the intrinsic wave number of propagating wave.) These numerical evidences strongly support our conjecture. We shall return this problem in further detail in the near future.

Acknowledgments

We would like to thank M. Tribelsky and V. Zykov for valuable discussions. This work was supported by the Grant-in-Aid for the 21st Century COE "Center for Diversity and Universality in Physics" from the Ministry of Education, Culture, Sports, Science and Technology (MEXT) of Japan.

---

[1] Y. Kuramoto: Chemical Oscillations, Waves and Turbulance (Springer-Verlag, Berlin, 1984).
[2] D. Walgraef: Spatio-Temporal Pattern Formation (Springer-Verlag, New York, 1997).
[3] M. C. Cross and P. C. Hohenberg: Rev. Mod. Phys. **65**, 851 (1993).
[4] T. Ohta: Physica D **151**, 61 (2001).
[5] (eds) A. Pikovsky and Y. Maistrenko: Synchronization: theory and application (Kluwer, London, 2003).
[6] A. von Oertzen, H. H. Rotermund, A. S. Mikhailov and G. Ertl: J. Phys. Chem. B **104**, 3155 (2000).
[7] Y. Tabe and H. Yokoyama: Langmuir **11**, 4609 (1995).
[8] R. Reigada, F. Sagues and A. S. Mikhailov: Phys. Rev. Lett. **89**, 038301 (2002).
[9] T. Okuzono, Y. Tabe and H. Yokayama: Phys. Rev. E. **69**, 050701 (2004).
[10] Y. Tabe and H. Yokoyama: Nature Materials **2**, 806 (2003).
[11] M. Lowe and J. P. Gollub: Phys. Rev. A **31**, 3893 (1985).
[12] P. Coullet: Phys. Rev. Lett. **56**, 724 (1986).
[13] C. W. Meyer, D. S. Cannell, G. Ahlers, J. B. Swift and P. C. Hohenberg: Phys. Rev. Lett. **61**, 947 (1988).
[14] P. C. Hohenberg and J. B. Swift: Phys. Rev. A **35**, 3855 (1987).
[15] H. Riecke, J. D. Crawford and E. Knobloch: Phys. Rev. Lett. **61**, 1942 (1988).
[16] V. Petrov, Q. Oyang and H. L. Swinney: Nature **388**, 655 (1997).
[17] K. Martinez, A. L. Lin, R. Kharrazian, X. Sailer and H. L. Swinney: Physica D **168-169**, 1 (2002).
[18] A. P. Muñuzuri, M. Dolink, A. M. Zhabotinsky and I. R. Epstein: J. Am. Chem. Soc. **121**, 8065 (1999).
[19] V. K. Vanag, A. M. Zhabotinsky and I. R. Epstein: Phys. Rev. Lett. **86**, 552 (2001).
[20] S. Rüdiger, D. G. Míguez, A. P. Muñuzuri, F. Sagués, and J. Casademunt: Phys. Rev. Lett. **90**, 128301 (2003).
[21] A. L. Lin, A. Hagberg, E. Meron and H. L. Swinney: Phys. Rev. E **69**, 066217 (2004).
[22] T. Okuzono and T. Ohta: Phys. Rev. E **64**, R045201 (2001).
[23] S. Sugiura, T. Okuzono, and T. Ohta: Phys. Rev. E **66**, 066216 (2002).
[24] T. Okuzono and T. Ohta: Phys. Rev. E **67**, 056211 (2003).
[25] S. Zykov, V. S. Zykov and V. Davydov: Europhys. Lett. **73**, 335 (2006).
[26] T. Ohta and H. Tokuda: Phys. Rev. E **72**, 046216 (2005).
[27] H. Tokuda and T. Ohta: to be published in Prog. Theor. Phys. Supple.
[28] P. Bak: Rep. Prog. Phys. **45**, 587 (1982).